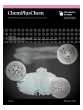

Looking for the Elusive Imine Tautomer of Creatinine: Different States of Aggregation Studied by Quantum Chemistry and Molecular Spectroscopy

Iker Léon[+],[a] Nicola Tasinato[+],[b] Lorenzo Spada[+],[b, c] Elena R. Alonso,[a] Santiago Mata,[a] Alice Balbi,[b] Cristina Puzzarini,*[c] Jose L. Alonso,*[a] and Vincenzo Barone*[b]

New spectroscopic experiments and state-of-the-art quantum-chemical computations of creatinine in different aggregation states unequivocally unveiled a significant tuning of tautomeric equilibrium by the environment: from the exclusive presence of the amine tautomer in the solid state and aqueous solution to a mixture of amine and imine tautomers in the gas phase. Quantum-chemical calculations predict the amine species as the most stable tautomer by about 30 kJ mol^{-1} in condensed phases. On the contrary, moving to the isolated forms, both Z and E imine isomers become more stable by about 7 kJ mol^{-1}. Since the imine isomers and one amine tautomer are separated by significant energy barriers, all of them should be present in the gas phase. This prediction has indeed been confirmed by high-resolution rotational spectroscopy, which provides the first experimental characterization of the elusive imine tautomer. The interpretation of the complicated hyperfine structure of the rotational spectrum, originated by three ^{14}N nuclei, makes it possible to use the spectral signatures as a sort of fingerprint for each individual tautomer in the complex sample.

Introduction

The conformational landscape of naturally occurring biomolecules is of great interest because structure-property relationships rule their functional specificity (see, for example, refs. 1–4 and references therein). Biomolecules exploit their functions in condensed phases where both intra- and inter-molecular interactions tune the overall behavior.[5] The disentanglement of the delicate balance between these two contributions is of paramount importance because it rules the specific structure-property characteristics of biomolecules and, ultimately, their activity. From this perspective, spectroscopic techniques are unique tools for non-invasively probing molecular systems in various environments, ranging from the condensed to the gas phase. Analysis and comparison of the signals obtained under different conditions can shed light on the subtle competition between intra- and inter-molecular contributions. However, two challenges must be addressed from an experimental point of view. First, for molecular species in condensed phases, only averaged properties can be derived and unraveling the different phenomena underlying the spectroscopic observables is difficult, if not impossible, when relying solely on experimental data. Second, while isolated molecules in the gas phase can be studied in great detail owing to the accuracy of high-resolution spectroscopic techniques, spectral analysis and interpretation are not at all straightforward because of several factors, such as spectral congestion, conformational relaxation and dynamical effects. State-of-the art quantum-chemical (QC) approaches are powerful tools to support experiment in these challenges. Indeed, they allow to get deeper insights into both the condensed and gas phase, provided that the computational model is able to correctly describe the fundamental chemical and physical properties of the investigated system.

In this work, a synergistic and integrated experiment-theory approach in the spectroscopy framework has been exploited to understand the physicochemical behavior of a biomolecule, creatinine. This involved performing the same experiments *in vitro* and *in silico*, thus leading to a journey among the aggregation states of this molecule: from the crystal, to the aqueous solution, to the isolated molecule in the gas phase. The effect of intra- and inter-molecular non-covalent interactions ruling the relative stability of creatinine tautomers in the different phases will be addressed, with the experiment-theory

[a] Dr. I. Léon,[+] Dr. E. R. Alonso, S. Mata, Prof. Dr. J. L. Alonso
Grupo de Espectroscopia Molecular (GEM),
Edificio Quifima,
Laboratorios de Espectroscopia y
Bioespectroscopia Parque Cientifico UVa
Universidad de Valladolid
47011 Valladolid (Spain)
E-mail: jlalonso@qf.uva.es
[b] Prof. Dr. N. Tasinato,[+] Dr. L. Spada,[+] A. Balbi, Prof. Dr. V. Barone
Scuola Normale Superiore
Piazza dei Cavalieri 7,
I-56126 Pisa (Italy)
E-mail: vincenzo.barone@sns.it
[c] Dr. L. Spada,[+] Prof. Dr. C. Puzzarini
Dipartimento di Chimica "Giacomo Ciamician"
Alma Mater Studiorum – Università di Bologna
Via Selmi 2, 40126, Bologna (Italy)
E-mail: cristina.puzzarini@unibo.it
[+] These authors contributed equally to this work.

Supporting information for this article is available on the WWW under https://doi.org/10.1002/cplu.202100224

approach being also supported by a vis-à-vis comparison between experimental and simulated spectral features.

Creatinine provides an excellent case study for this integrated strategy not only because of its biochemical relevance (vide infra), but also because its complicated potential energy surface (PES) has not been completely understood yet and its gas-phase behavior is still unexplored from the experimental point of view. In the latter respect, rotational spectroscopy plays a central role in determining accurate molecular structures[6–9] for all low-energy tautomers, isomers, and conformers separated by barriers sufficiently high to avoid interconversion.[10–16] However, the interpretation of spectroscopic data for large flexible systems is a daunting task because of the concomitant presence of different species and several strongly interconnected parameters. In such a situation, an experiment-theory approach is unavoidable, with the support of QC calculations being fundamental for guiding experiments and interpreting the acquired spectra, provided that accurate state-of-the-art methodologies are employed.[7–10,17–19]

Concerning the specific topic of this work, creatine phosphate is used to convert adenosine diphosphate to adenosine triphosphate[20] in human skeletal muscle tissue. In a side reaction, creatinine is a breakdown product of creatine phosphate, which is almost exclusively eliminated through the kidney in the urine. High blood levels of creatinine are thus a symptom of kidney filtering disorders; therefore, this molecule can be used as an indicator of renal health.[20–22] More generally, creatinine concentrations in the blood and urine can be employed as indicators of renal dysfunction, muscle pathologies, and early detection of myocardial infarction.[20,22] According to a recent classification system by the Acute Dialysis Quality Initiative, acute kidney injuries can be indeed pointed out by percentage increases in serum creatinine over baseline.[23] Furthermore, creatinine is in equilibrium with creatine,[24] this latter being partially formed from the former in neutral and alkaline solutions.

In view of the importance of creatinine highlighted above, several studies have been devoted to the investigation of its structural properties, with those focusing on the isolated molecule being very limited. Indeed, a few theoretical investigations have been carried out, which cannot, however, be considered at the state of the art according to current standards[7] because they are based on semiempirical models,[25,26] second-order Møller-Plesset perturbation theory (MP2), or density functional theory (DFT), employing in the latter two cases rather small basis sets.[27,28,29] All these works suggest that, in the gas phase, the imine tautomer (**I**, see Figure 1) is slightly more stable than the amine form (**A**, obtained by the migration of H10 from N3 to N6; see Figure 1 for labelling). On the other hand, NMR and Raman studies suggest that only the amine form is present or, at least, strongly favoured in polar solvents.[25,26,28,30] The same applies to the solid state according to the most recent X-ray diffraction study[31] that rectifies the older interpretation in terms of the imine tautomer[32] (also employed, without any justification, in a recent Raman investigation[33a]). Enolic tautomers are also possible, which can be obtained either from the migration of

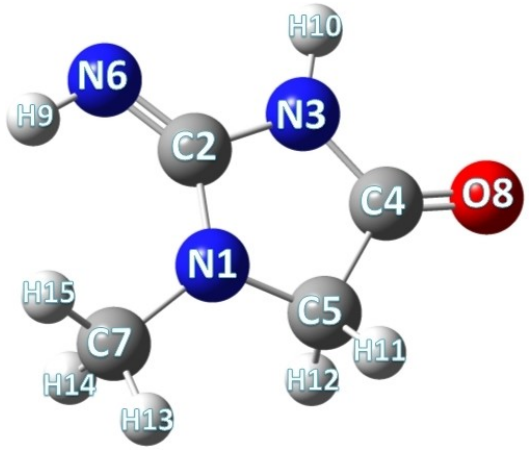

Figure 1. Structure and atom numbering of the imine tautomer of creatinine.

H10 from N3 to O8 (Hy) or the migration of H11 (or H12) from C5 to O8, in this latter case starting either from imine (**IH**) or amine (**AH**) tautomers.[29] Furthermore, E and Z isomers are possible for the imine moiety (labeled **EI** and **ZI**, respectively). We are thus left with the eight structures shown in Figure 2. The splitting of enol and amine tautomers in pairs of close-lying isomers (referred to, in the following, as **E** and **Z** for enols, and **A1** and **A2** for amines) is also possible due to the OH rotation and the NH_2 inversion, respectively. Therefore, a total of 16 energy minima is expected if we only consider tautomers that do not involve any charge separation in the standard Lewis structure. Noted is that for IH and IHy forms, the specification of **Z** or **E** isomerism of the enol moiety follows that of the imine moiety (e. g. **EZIH** or **ZEIHy**).

From an experimental point of view, no data are available in the gas phase and some of the spectra in the solid state are not sufficiently resolved. For this reason, we have decided to perform a comprehensive rotational (microwave) study in the gas phase and to record new infrared (IR) spectra in the solid state. As mentioned above, previous computational results are fragmentary and not sufficiently accurate for the assignment and interpretation of spectral features. Therefore, to support the experimental investigation, we have studied the tautomeric behaviour of creatinine over different aggregation states by means of state-of-the-art computations, thereby properly including stereo-electronic, vibrational (also incorporating anharmonicity), and environmental (either periodicity in solids or integrating the first solvation-shell together with the proper account of the bulk in solution) effects.

Results and Discussion

On the basis of previous experience,[7,34,35,36] the QC computations have been performed with the global hybrid B3LYP functional[37] in conjunction with a double-ζ basis set (hereafter B3) or the double-hybrid B2PLYP functional[38] in conjunction with a triple-ζ basis set (hereafter B2), in both cases taking into

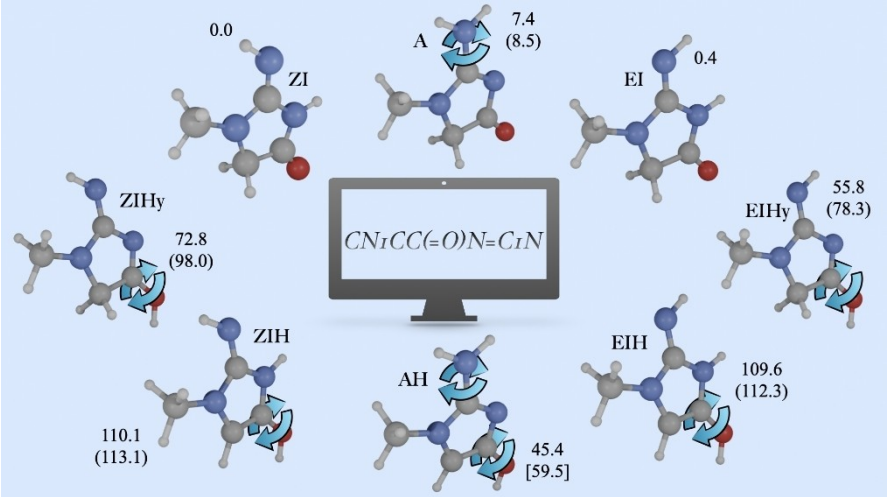

Figure 2. Starting from the SMILE (Simplified Molecular Input Line Entry System) chemical notation inside the computer screen, the eight possible structures of creatinine are shown, with the corresponding B2 relative energy being also reported. Eight additional structures can be obtained, as highlighted by the arrows, by NH_2 inversion and/or OH rotation (for instance, the **A** form is split into **A1** and **A2**, whereas the **EIHy** form is split into **EZIHy** and **EEIHy**), with the corresponding B2 energies being provided within parentheses. Different Z-imine isomers are shown on the left and the corresponding E-imine isomers on the right (I, IHy and IH from top to bottom). For the **AH** form (bottom structure), two nearly degenerate orientations of the OH bond are possible (their averaged energy is provided in brackets). All the energies are in kJ mol^{-1}.

account dispersion contributions using the D3BJ model.[39] More accurate estimates have been obtained employing the so-called 'cheap' composite scheme (hereafter ChS)[40] or the CCSD(T)-F12[41] method in conjunction with the cc-pVDZ–F12[42] basis set (hereafter CCDZF12). Further information is provided in the section devoted to computational details, while a complete account can be found in the Supporting Information (SI).

In Figure 2, together with the possible tautomers and isomers of creatinine, the relative energies are also reported. These confirm that, as previously suggested,[27–29] enolic forms are significantly less stable than their ketonic counterparts. Therefore, their contribution is surely negligible in all aggregation states and will not be considered in the following.

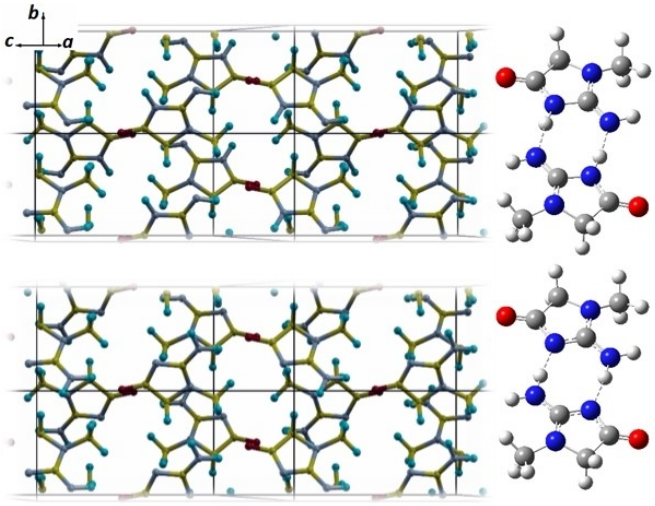

Figure 3. Left panels: Computed crystal structures of the creatinine imine-tautomer (top) and amine-tautomer (bottom). Right panels: Geometries for the creatinine imine tautomer (top) and amine tautomer (bottom) dimers.

The solid state

According to the available experimental investigations,[31,32] the creatinine crystal belongs to the P21/c space group and it contains four molecules per unit cell. The B3 optimized crystal structures of the imine and amine tautomers of creatinine are shown in Figure 3 (left panels), while Table 1 and Table S1 of the SI report the relevant computed geometrical parameters and compare them with available experimental data. The only significant differences in the cell parameters of the two tautomers (see Table 1) are observed for the *c* axis and the β angle. Concerning atomic positions, the parameters showing significant differences between the structures of the two tautomeric forms are collected in Table S1.

In the original X-ray study,[32] which dates back to 1955, it was not possible to identify the position of the hydrogen atoms, thus leaving the question on the presence of the imine and/or amine tautomer unaddressed. A more recent investigation[31] demonstrated that only the amine form is present in the crystal, however providing *c* and β cell parameters significantly different from those of the previous study, as can be appreciated in Table 1. Two different computational approaches (both incorporating periodic boundary conditions) have been adopted to elucidate such inconsistency. In the first one (Theo1), the cell parameters have been kept fixed at the values of ref. [31] and only atomic coordinates have been optimized. In the second one (Theo2), both cell parameters and atomic positions have been relaxed. Irrespective of the two approaches, computations indicate that the crystal of creatinine in the amine form is more stable than the imine counterpart (by 107.3 kJ mol^{-1} from Theo2; 149.3 kJ mol^{-1} from Theo1). Taking into account that

Table 1. Computed and experimental cell parameters (in Å and degrees) and relative stability (in kJ mol^{-1}) of crystals for the imine and amine creatinine.

	Theo1[a] [amine]	Theo1[a] [imine]	Theo2[b] [amine]	Theo2[b] [imine]	Exp1[c]
a	8.015	8.015	7.522	7.519	8.015/8.06
b	5.926	5.926	5.605	5.570	5.926/5.97
c	11.419	11.419	13.063	13.270	11.419/13.34
β	96.25	96.25	123.93	124.59	96.25/121.0
ΔE	0.0	149.3	0.0	107.3	–
ΔE/molecule	0.0	37.3	0.0	26.8	–

[a] Cell parameters fixed to the experimental values of ref. [31]. [b] Cell parameters from full geometry relaxation. [c] Experimental parameters: ref. [31] / ref. [32].

there are four molecules in the unit cell, the stabilization brought by one single amine molecule over the imine one can be estimated to be 26.8 kJ mol^{-1} (Theo2; 37.3 kJ mol^{-1} from Theo1). Hence, only the amine tautomer should be found in the solid phase.

Despite this result, contradictory interpretations of the vibrational spectra of the solid compound have been reported in the literature.[33] In ref. [33b], the IR spectrum has been analysed in terms of the amine tautomer, but two years later,[33a] the imine form has been considered for explaining the Raman features. To solve this issue, IR spectra of both the imine and amine crystals have been computed at the B3 level within the double-harmonic approximation, and compared with a new experimental spectrum, purposely recorded (see Experimental details). As shown in Figure 4 (panels **a** and **b**), QC simulations unequivocally lead to the interpretation of the IR spectrum in terms of the amine form. Indeed, the features in the 1500–1650 cm^{-1} region are well explained in terms of the NH_2 bending vibrations of the amine tautomer, while the simulation of the imine IR spectrum does not show transitions in that range. A second fingerprint region is around 3000 cm^{-1}, where – according to our computations – the absorptions at

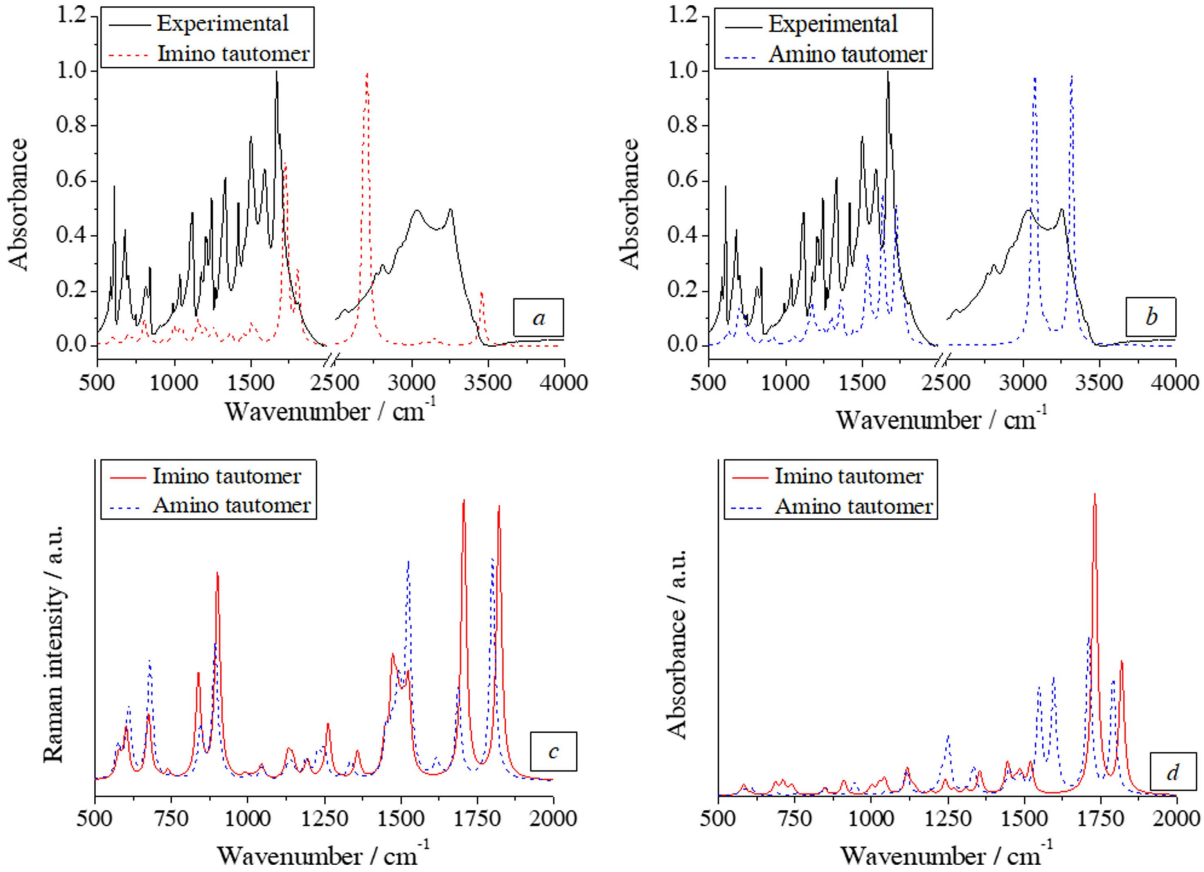

Figure 4. Top panels: Experimental IR spectrum (between 500 and 4000 cm^{-1}) of the creatinine crystal in KBr pellet: comparison with the simulated counterpart obtained for the imine (a) and amine (b) crystal structures within the double-harmonic approximation adopting a periodic approach. Bottom panels: Raman (c) and IR (d) spectra of the creatinine homo-dimers in the 500–2000 cm^{-1} computed at the B3 level within the double-harmonic approximation.

3253 cm^{-1} and 3033 cm^{-1} can be ascribed to the symmetric and antisymmetric NH_2 stretching vibrations of the amine group, respectively. Conversely, the simulated IR spectrum of the imine tautomer presents a single intense band at about 2707 cm^{-1} and a medium-intensity absorption around 3457 cm^{-1}, both incompatible with the observed band shape.

In the framework of the analysis of the vibrational spectra of solid creatinine, different dimers of creatinine, as models of the periodic motif within the crystalline lattice, have been theoretically investigated in ref. [33a], with only the imine-tautomer dimers being however considered. In that work, starting from these imine dimers, the Raman spectrum was simulated at the harmonic level and used to interpret the experimental one. However, the ground state energies computed in the present study for the dimers of the amine and imine tautomers unequivocally show that the former is more stable than the latter by 8.3 kJ mol^{-1}, further confirming the outcomes discussed above in the context of periodic calculations.

Simulations of the vibrational spectra of the creatinine crystal based on model dimers deliver only qualitative results due to the lack of some intermolecular interactions present in the molecular crystal (in particular those affecting the carbonyl group) and the stacking of creatinine units. Despite their limitations, these simplified models can anyway provide useful atomistic interpretations. We have, therefore, optimized the geometry of the homodimer of the **ZI** and **A1** tautomers (see Figure 3, right panels) and then computed the corresponding Raman and IR spectra (Figures 4c and 4d) as described in the computational details section. The Raman spectra of the imine and amine homodimers are similar in the 500–2000 cm^{-1} range, i.e., the same fingerprint region targeted in ref. [33a]. Instead, in analogy with periodic QC computations, the IR spectra differ for the presence of the NH_2 bending modes for the dimer of the amine form.

The aqueous solution

We have next investigated the aqueous solution of creatinine employing the so-called clusters-in-a-liquid model[43]. In details, the structures of creatinine tautomers (and the transition state ruling their interconversion) plus their first solvation-shell (see Figure 5) have been optimized at the B2 level, with bulk solvent effects described by the polarizable continuum model (CPCM). Preliminary molecular dynamics simulations agree on an average number of 5 water molecules in the first solvation shell of creatinine. The clusters-in-a-liquid computations point out that the interconversion from the two tautomers occurs by a relay mechanism in which two water molecules play the role of "bridge" for the proton transfer. Adducts incorporating only the two "bridge" molecules were already analyzed in ref. [29], and provided a reasonable model. However, we preferred to investigate in detail a 5 W model in which two further water molecules interact with the lone-pairs of the carbonyl oxygen, and the fifth molecule forms a hydrogen bond with the outer hydrogen atom of the amine or imine group. Our computations indicate that in aqueous solution, the amine tautomer (**A1**) is more stable by about 30 kJ mol^{-1} than its imine counterpart (**ZI**) and that the first-shell and bulk solvent effects play comparable roles in determining the overall stability order. The bulk effect is easily explained in terms of the much larger dipole moment of the amine tautomer (7.73 vs. 3.61 D for the isolated molecule at the B2 level), whereas the further relative stabilization of the amine isomer by interaction with the first-shell solvent molecules is due to an interplay of electrostatic, dispersion, and steric contributions.

The relative stability of the amine and imine tautomers obtained in aqueous solution is in nice agreement with that computed for the molecular crystal, thus suggesting that intermolecular hydrogen bonds stabilize the amine tautomer over the imine one, whereas it can be anticipated that the intramolecular interactions favour the imine form (see the discussion for the gas phase).

From the experimental point of view, NMR data agree with the exclusive presence of the amine form.[26,30] On the contrary, based on harmonic DFT computations,[28] Raman spectra have been interpreted in terms of contributions from both tautomers. In order to solve this controversy, we have re-investigated the Raman spectrum by coupling harmonic B2 computations with B3 anharmonic contributions, for both frequencies and intensities, in the framework of the generalized second-order vibrational perturbation theory (GVPT2).[44,45] The computed Raman spectrum for the **A1-5 W** model (see Figure 5) embedded in a polarizable continuum is compared, in Figure 6,

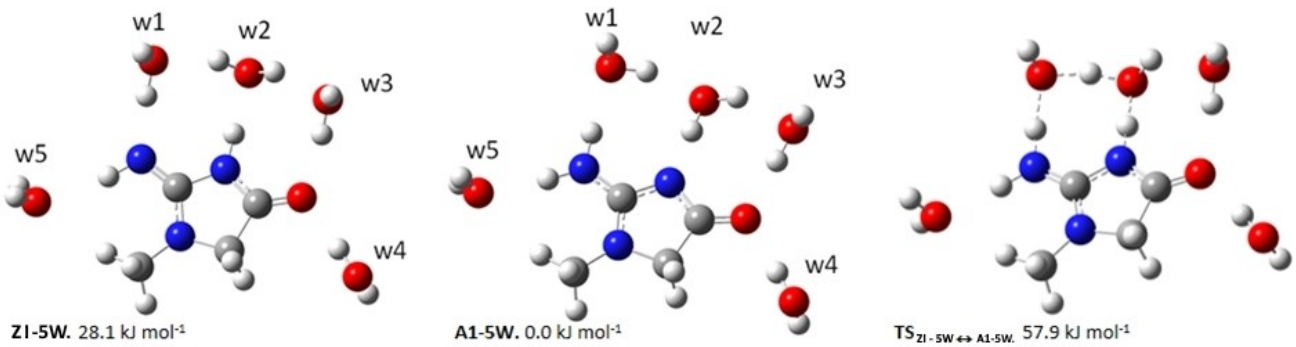

Figure 5. Creatinine complexed by five water molecules. Left: imine-tautomer 1 (**Z1-5 W**). Middle: amine-tautomer 3 (**A1-5 W**). Right: the transition state connecting imine and amine tautomers. The relative stabilities include bulk solvent effects taken into account at the CPCM level.

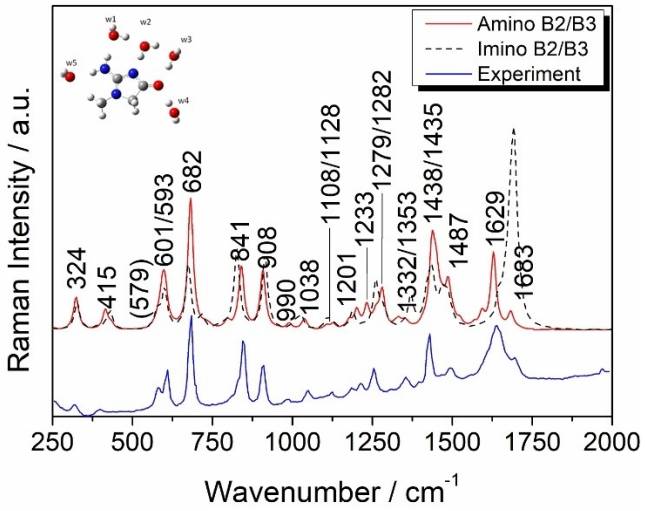

Figure 6. Comparison between the experimental Raman spectrum and the anharmonic B2/B3 counterpart of the imine and amine tautomers of creatinine in aqueous solution (between 250 and 2000 cm^{-1}). The most relevant absorptions are labelled. The simulated band-shape spectrum has been obtained by convolving the computed stick-spectrum with a Lorentzian function with a half-width at half-maximum of 10 cm^{-1}.

with the experimental counterpart reported in ref. [28]. The latter was recorded at pH = 7, thus creatinine is expected to be in a neutral form.

The vis-à-vis comparison between simulated and experimental spectra (Figure 6) shows a remarkable agreement for both specific bands and the overall spectral shape. A detailed assignment is given in Table 2, where a nice 1:1 correspondence between computed and recorded features is apparent. This comparison confirms that only the amine tautomer is present in aqueous solution without any need to invoke contributions from the imine form, as done instead in ref. [28]. Indeed, the scaled harmonic computations employed in ref. [28] for spectral assignments cannot account for the contributions arising from overtones and combination bands, do not reproduce intensity alterations due to electrical anharmonicity, and completely neglect anharmonic resonances. The present results instead fully reconcile theory and experiment and rule out any role of the imine tautomer in polar solvents, which would be hardly explainable in view of its predicted much lower stability and the high barrier to interconversion.

Table 2. Hybrid B2/B3 anharmonic vibrational wavenumbers of the amine tautomer of creatinine in aqueous solution compared to experimental data. Values in cm^{-1}.

Simulation[a]	Experiment [pH = 7][b]
324 (ν_{35})	320
415 (ν_{34})	397
593 (ν_{32})/579(ν_{33})	580
601 (ν_{31})	605
682 (ν_{29})	682
841 (ν_{26})	845
908 (ν_{25})	905
990 (ν_{24})	982
1038 (ν_{23})	1048
1128 (ν_{21})	1122
1178 ($2\nu_{30}$)	1186
1233 (ν_{19})/1201 (ν_{20})	1216
1279 (ν_{17})/1262 (ν_{18})	1256
1353 (ν_{16})/1332 ($\nu_{28}+\nu_{30}$)	1353
1407 ($\nu_{27}+\nu_{29}$)	1396
1435 (ν_{15})/1438(ν_{14})/1449(ν_{13})	1428
1487 (ν_{11})	1493
1629 (ν_{9})	1641
1683 (ν_{8})	1697

[a] The main transitions contributing to the band are within parentheses. [b] Ref. [28].

The role of different solvent molecules belonging to the first solvation shell in tuning the tautomeric equilibrium of creatinine is shown in Figure 7 together with the additional contribution provided by the bulk solvent effect. Starting from the **5 W** adducts shown in Figure 5, water molecules are removed (from right to left in Figure 7) in the order w5, w4 + w3, w2, and w1 (for the labeling of water molecules, see Figure 5). It is apparent that removing the water molecule bound to outer aminic or iminic hydrogen (w5) and to the carbonyl group (w3, w4) leads to nearly isoenergetic imine and amine adducts with 2 water molecules (**2 W**), with the amine form remaining more stable by about 3 $kJ\,mol^{-1}$. Finally, removal of one (w2) or both the two last (w2 + w1) molecules leads to a marginally more stable imine form, thus suggesting that both tautomers might be present in the gas phase.

In fact, the atomistic details of the complex formed by creatinine and two water molecules point out that, as in the case of the homodimers, the occurrence of two intermolecular hydrogen bonds is sufficient to tip the scales in favor of the amine tautomer. According to the discussion above, only the amine tautomer can be characterized in polar solvents.

The gas phase

Finally, we turn our attention to the isolated molecule (gas phase). In the previous section, it has been shown that by

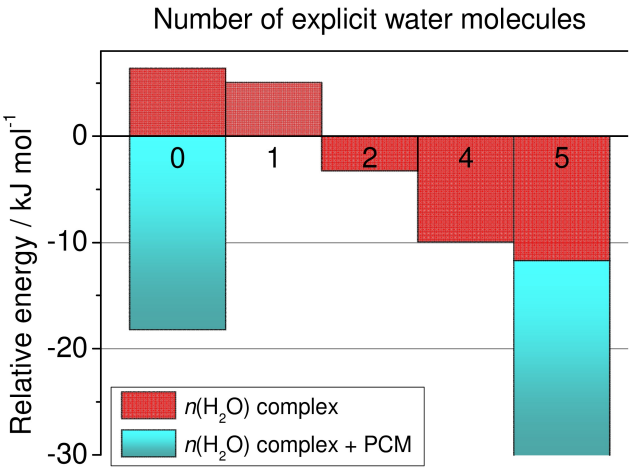

Figure 7. Relative stability of the most stable imine (**ZI**) and amine (**A1**) tautomers as a function of the number of water molecules directly bonded to creatinine (red) and of bulk solvent effects (cyan, estimated by means of CPCM). Positive values indicate that the imine tautomer is more stable.

removing the water molecules of the first solvation shell the stability order can be reversed; for the isolated species, the imine form could become the most stable. Therefore, a comprehensive study of isolated creatinine integrating state-of-the-art QC computations and microwave spectroscopy has been carried out to characterize this elusive tautomer. In this respect, we recall that creatinine contains three nitrogen atoms. The latter being quadrupolar nuclei (i.e. nuclear spin $I=1$, in the present case), the rotational spectrum shows a complex hyperfine structure, which is further complicated by the presence of a methyl group that undertakes an internal rotation motion. Such a complexity is further enhanced by the flexibility of the system that leads to the concomitant presence of several conformers and tautomers. Therefore, the investigation of isolated creatine represents a challenging task, from both an experimental and computational perspective.

The QC exploration of the creatinine PES at the B2 level identified the 16 energy minima shown in Figure 2 (where the corresponding B2 relative energies are also reported). A detailed analysis of the PES, also including the transition states ruling the interconversion between the different tautomers that do not involve CH bond breakings, is provided in Figure S1 of the SI and the relative energies of the transition states are collected in Table S3 (the energies of all minima are instead given in Figure 2). The PES can be ideally divided into two regions (see Figure S1). The low-energy portion includes the **ZI**, **EI**, **A1** and **A2** (1, 2, 3, and 4 in Figure S1) minima, which are the isomers of relevance to the gas-phase spectroscopic investigation. They are separated by high-energy barriers from the high-energy region of the PES that contains all HN isomers (5, 6, 7 and 8 in Figure S1), whose relative energies range between 55 and 98 kJ mol^{-1} (above the global minimum). The structures and relative energies of the transition states (TSs) governing interconversion between the four lower-energy minima are sketched in Figure S2 of the SI together with their relative B2 energies, while the structures and energies of all the other TSs are given in Figure S3 of the SI.

The best estimates of equilibrium (ΔE_{el}) and ground-state ($\Delta E_0 = \Delta E_{el} + \Delta$ZPE, ZPE standing for anharmonic zero-point energy at the B3 level) relative energies of the main stationary points located on the low-energy part of the PES are collected in Table 3 and, for a complete list, in Table S4 of the SI. In these tables, the B2 results are compared with those issuing from the accurate ChS QC protocol (described in detail in the SI). The excellent agreement between B2 and ChS relative energies allows us to point out the reliability and accuracy of the B2 model for energetic studies, thus giving further support to the energetics worked out for the aqueous solution.

Table 3. Equilibrium and ground-state relative energies [kJ mol^{-1}] of the low-lying creatinine isomers and the transition states ruling their interconversion.

Structure	ΔE^{el} B2[a]	ΔE^{el} ChS[b]	$\Delta E^{0\ Anh}$,[c]
ZI	0.0	0.0	0.8
EI	0.4	0.2	0.0
A1	7.4	7.7	7.6
A2	8.5	9.3	9.9
TS(**ZI-EI**)	80.5	85.2	80.1
TS(**ZI-A1**)	205.3	207.2	191.8
TS(**A1-A2**)	8.6	9.5	8.2

[a] Electronic energy at the B2 level. [b] ChS electronic energy. [c] Ground-state energy: ChS electronic energy augmented by anharmonic B3 ZPE.

Referring to the bare electronic energy of the isolated system, it is noted that the global minimum of the PES, **ZI** (1), is almost iso-energetic with EI (2), which lies only 0.2 kJ mol^{-1} higher in energy. These are followed by **A1** (3) and **A2** (4) with a relative electronic energy of 7.7 and 9.3 kJ mol^{-1}, respectively. However, when ZPE is included, the stability order of **ZI** and **EI** is reversed, with the **EI** isomer being more stable by 0.8 kJ mol^{-1} than **ZI**. The TS ruling the interconversion between these two forms lies at high energy (about 80 kJ mol^{-1}) and this is also the case for conversion between **ZI** and **A1** (207 kJ mol^{-1}). Different is the situation for the two amine isomers. Indeed, after the inclusion of the ZPE correction, the TS linking **A1** and **A2** lies below **A2**. This means that **A2** relaxes to **A1**, which is – therefore – the only amine tautomer suitable for the experimental observation together with both the imine species, **EI** and **ZI**. While full details about these processes are given in the SI, we only mention that, from the inspection of Figure S1b, it is noted that for minima and most of the TSs, couples of isomers are present. In each case, these equivalent minima lie at the bottom of a double-well potential, and are usually separated by small energy barriers. It is worth noticing that their interconversion cannot be described as a simple rotation of the methyl group, but rather it is a complicated path involving both the CH_3 rotation and the inversion of the corresponding nitrogen atom. Moving to the spectroscopic characterization, the equilibrium rotational constants are straightforwardly obtained from the B2 equilibrium geometries. To improve the estimated rotational constants, the structures of the **EI**, **ZI**, and **A1** isomers have also been optimized at the higher CCDZF12 level of theory (see computational details). The resulting rotational constants are collected in Table 4. Their comparison with the B2 counterparts points out an excellent agreement, thus confirming –once again– the accuracy and reliability of the latter level of theory. However, to predict the experimental features, we need to move from the bottom of the well to the vibrational ground state. The same also applies to other spectroscopic parameters, such as the nuclear quadrupole-coupling constants. Vibrational corrections to both types of constants were obtained at the B3 level in the framework of the GVPT2 model.[44,45] The rotational and quadrupole-coupling constants, for all energy minima, are given in Tables S5 and S6, respectively.

As detailed in the Experimental section, two different Fourier transform microwave (FTMW) spectrometers have been employed for the experimental investigation. The first spectral recordings were performed using the LA-CP-FTMW spectrometer,[46–48] globally covering the 2–18 GHz range. An example is shown in Figure 8a, where the rotational spectra have been obtained with three different polarization powers. These consist of several rotational transitions, also highlighting not well-resolved hyperfine structures due, as already mentioned, to the presence of three ^{14}N nuclei. Even if not entirely resolved, the hyperfine structures helped us to confirm that the

Table 4. Comparison between experimental and quantum-chemical spectroscopic parameters for the **A1**, **ZI** and **EI** creatinine isomers.

		A1		**ZI**		**EI**		
		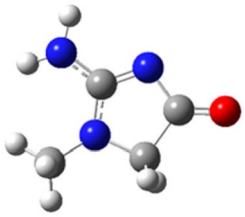		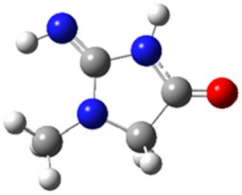		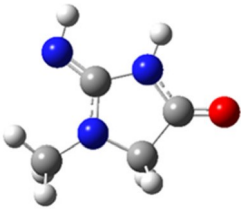		
		Experiment[a] State A	Theory[b]	Experiment[a] State A	Theory[b]	Experiment[a] State A	State E	Theory[b]
A_0		3840.94750(60)	3812.0 (3801.4)	3842.39445(57)	3803.3 (3807.1)	3890.1584(19)	3888.07(82)	3864.4 (3871.9)
B_0		1831.49589(28)	1817.9 (1820.3)	1825.35305(16)	1813.5 (1813.5)	1810.31700(27)	1810.189(45)	1797.9 (1797.3)
C_0		1266.86054(25)	1256.5 (1264.6)	1261.00347(14)	1250.8 (1255.6)	1258.07095(26)	1258.066(45)	1247.7 (1252.6)
N1[c]	χ_{aa}	2.4309(21)	2.451	2.7371(14)	2.792	2.7073(37)		2.713
	χ_{bb}	2.4582(30)	2.486	2.6260(17)	2.645	2.6075(42)		2.622
N3[c]	χ_{aa}	2.0011(31)	2.011	1.8672(21)	1.839	1.9027(57)		1.835
	χ_{bb}	−2.3972(26)	−2.547	1.6862(24)	1.643	1.8035(59)		1.883
N6[c]	χ_{aa}	2.0088(36)	2.083	1.9194(17)	1.945	−2.1750(27)		−2.296
	χ_{bb}	1.9158(33)	1.976	−2.3675(15)	−2.380	1.8326(44)		1.917
D_a [d]							−56.08(69)	
D_b [d]							−14.793(80)	
$\lvert\mu_a\rvert$ [c] [D]			7.51		2.28			0.98
$\lvert\mu_b\rvert$ [c] [D]			1.82		2.79			0.59
$\lvert\mu_c\rvert$ [c] [D]			0.26		0.14			0.22
N° of lines		113		160		125		
σ [kHz]		2.2		2.2		2.5		

[a] All parameters, except otherwise stated, are in MHz. Estimated accuracy for frequency measurements: 3 kHz. Standard errors (1σ) in units of the last quoted digits of the value of the rotational parameter. [b] Ground-state rotational constants were obtained by adding B3 vibrational corrections to B2 or CCDZF12 (within parentheses) equilibrium values. [c] Ground-state dipole moment components (absolute values) and quadrupole coupling constants obtained by adding B3 vibrational corrections to B2 equilibrium values. [d] Torsion-rotation interaction parameters (according to ref. [55], negative values of these parameters have been enforced. Noted is that the signs of D_a and D_b are not determinable from the fit).

assigned lines belong to creatinine species. No attempt was initially made to analyse them, but rather the centres of the corresponding hyperfine pattern were measured and fitted to a rigid-rotor Hamiltonian.[49] According to the computed dipole moment components (see Table 4), the μ_a-type transitions are well suited for discriminating among the various species. Therefore, for each transition, several experiments were performed adjusting the microwave polarization power (according to the dipole moment value) in order to ensure a fast linear passage (LFP) regime condition. A portion of the corresponding spectra, recorded with decreasing microwave polarization powers (from black to blue spectra), is shown in Figure 8b (3060-3110 MHz range). From the bottom to the top, i.e. going from the lowest to the highest power attenuation, useful information on the isomeric assignment can be deduced. In fact, in agreement with the predicted values of the μ_a dipole moment component of the various species, the 1_{01}-0_{00} rotational transition of the **EI** isomer reaches the maximum signal-to-noise ratio (S/N) when the lowest attenuation is used (black trace), while some transitions of **ZI** and **A1** are depleted due to multi-resonance effects.[50,51] On the other hand, lowering the microwave polarization power, the 1_{01}-0_{00} transition of the **ZI** and **A1** species become observable, then reaching the maximum S/N at the highest power attenuation (blue trace). However, at this stage, it is not possible to definitively assign the tautomer because both frequency values and intensities are consistent with both **ZI** and **A1**. In fact, the predicted rotational constants are similar, and the same applies to the expected intensities because of a compensation between population and magnitude of the dipole moment along the *a*-axis (see Tables 3 and 4). Furthermore, Figure 8 allows us to point out the complexity of the present work: the population is split into three species, the overall intensity of each rotational transition is spread over many hyperfine components and, as can be seen in Figure 8c for **EI**, each rotational transition is also split into two states (A and E) due to internal rotation (see below). The other two isomers, **A1** and **ZI**, also display splittings due to the internal rotation of the methyl group. However, the V_3 parameters are not determined due to the limited number of E components observed in the recorded frequency range. After the μ_a-type transitions were used to obtain an initial fit, the investigation was extended to μ_b-type transitions and, using different attenuation powers, the weak features of the **EI** species could also be successfully observed and assigned. The experimental rotational constants derived at this stage are in line with their computed counterparts, with the difference between the *A* rotational constant of **EI** and those of the other two species (about 50 MHz) being well reproduced (see Table 4). Once the rotational spectra of the three species were confidently assigned, they have been investigated at higher

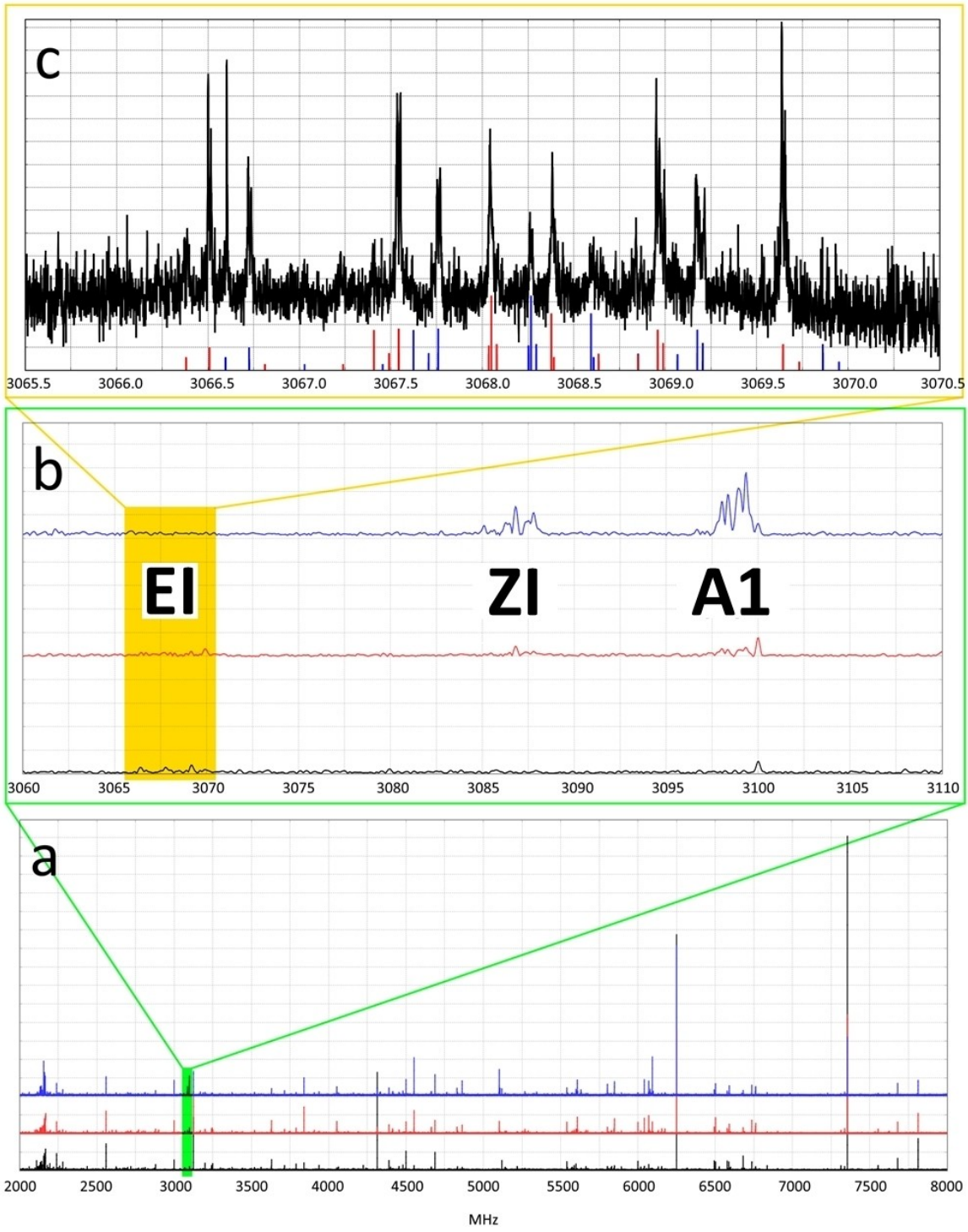

Figure 8. a) The LA-CP-FTMW recorded spectra using decreasing power-attenuation values in the 2–8 GHz range. Each spectrum (from black to blue) was recorded using a successive decrease in the polarization power of 5 dB (~75% decrease). b) The LA-CP-FTMW spectra magnification in the 3060–3110 MHz range of the portion highlighted in green in (a), also reporting the labelling of the observed isomers. c) The LA-MB-FTMW recorded spectrum for **EI** species in the 3065.5 – 3070.5 MHz range, also showing the hyperfine and internal rotation pattern predictions (E state in red, A state in blue).

resolution with the LA-MB-FTMW spectrometer[16,52,53] in the overall 2–18 GHz frequency range. This allowed for unveiling the characteristic hyperfine structures, which are collections of unique nitrogen quadrupole-coupling fingerprints of the observed molecular species. As an example of the resolution obtained in the LA-MB-FTMW recordings, in Figure 9, the hyperfine components of the 1_{11}-0_{00} rotational transition of the **ZI** and **A1** species are compared to the predictions issuing from the fits performed using the VMS-ROT software,[54] which is interfaced with the SPFIT program.[49] In this connection, the

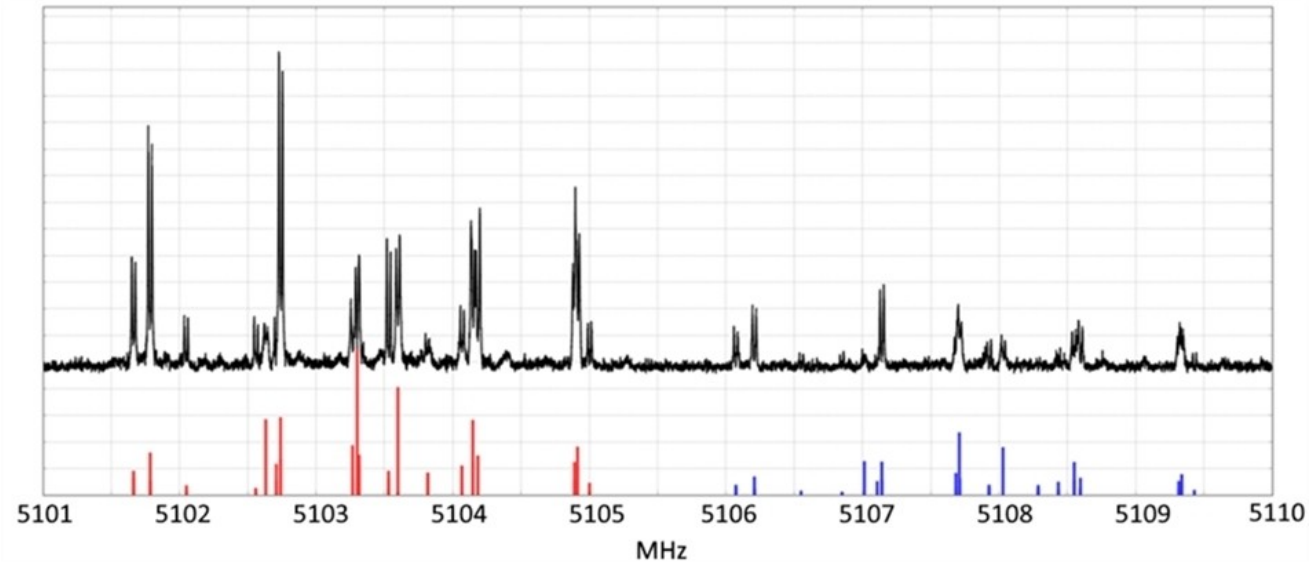

Figure 9. The 1_{11}-0_{00} rotational transition of the **ZI** (5101.5-5105.5 MHz range) and **A1** (5106-5109.5 MHz range) species recorded using the LA-MB-FTMW spectrometer, together with the corresponding spectral simulations (in red for **ZI**, in blue for **A1**). Each hyperfine component is split by the Doppler effect.

computed values of the nuclear quadrupole-coupling constants (see Table 4 and Table S6 of the SI) have the required accuracy to allow the assignment of spectral lines and provide reliable starting values for their fitting. Furthermore, these parameters – together with rotational constants – allow for discriminating among the different species. In fact, while the quadrupole-coupling constants of N1 are similar for all isomers, those of N3 are quite different for the imine and amine forms, and the absolute values of the χ_{aa} and χ_{bb} components of N6 are inverted on going from **EI** to the **ZI** isomer.

No attempt to estimate the relative abundances using the intensity of the rotational transitions was done because of potential factors affecting the final populations. As an example, the population of the **A1** tautomer was estimated larger than the predicted one. A reason could be that some of species populated before the supersonic expansion interconvert into the most stable species after the cooling process, altering the final abundances. Another source of error is the population potentially being perturbed from the original crystal species, as well as kinetic/thermodynamic effects during the supersonic expansion can contribute to alter the population ratio. Taking all these facts into account, we chose not to estimate the population ratios.

The final experimental spectroscopic parameters are collected in Table 4, where they are compared with their QC counterparts. The good agreement mentioned above is indeed observed, thus demonstrating the accuracy and suitability of the chosen computational approach. Since both rotational and quadrupole-coupling constants are strongly related to the molecular structure,[7,8,56] such a good agreement is also an indirect demonstration of the accuracy of the B2 structural determinations, further supported by CCDZF12 calculations. Therefore, the joint experimental-theoretical investigation of the isolated molecule, while confirming the reliability and accuracy of the B2 computational model, benchmarks the results obtained for the transition from the gas phase to the aqueous solution as well as for the characterization of creatinine in condensed phases.

Conclusions

In this work, different spectroscopic techniques have been exploited for each aggregation state to obtain those experimental data that are relevant for providing information on the behavior of creatinine. The *in vitro* measurements have been paralleled by *in silico* experiments tailored for the specific aggregation state considered, thus allowing us to perform a vis-à-vis comparison of the experimental and calculated spectroscopic features, with the final aim of unveiling the underlying structural and physical-chemical properties.

At first, the structural and vibrational spectroscopic properties of the molecular crystal have been simulated by means of periodic DFT computations, which are able to provide an unequivocal interpretation of the IR spectra recorded experimentally and to clarify some contradictory pieces of information reported in the literature. The overall conclusion is that, in this phase, the amine tautomer is strongly favored.

Next, the already available experimental Raman spectra of creatinine in aqueous solution have been computed by adopting a mixed discrete-continuum model for the solvent. The remarkable agreement between theoretical and experimental band-shapes has led to the conclusion that only the amine tautomer is present in aqueous solution, as also suggested by the computed energetics for the tautomerization reaction. Then, a detailed analysis of micro-solvation effects has been carried out by removing step-by-step the water molecules of the first solvation shell, thus concluding that in the condensed

phases two intermolecular hydrogen bonds favor the stability of the amine over the imine. However, for the 1:1 creatinine-water complex, the stability order is reversed, and for the isolated molecule the imine tautomer is predicted to be more stable than the amine analogue. A detailed exploration of the PES for the isolated molecule, carried out by coupling DFT and state-of-the-art wavefunction-based QC methods, has laid the foundation for the interpretation of the rotational spectra of creatinine in the gas phase. In this respect, a rotational spectroscopy study in supersonic expansion has succeeded in unequivocally detecting the elusive imine tautomer together with the amine species despite the great complexity of the rotational spectra. This is related to the concomitant presence of different species as well as to the hyperfine structure due to three nitrogen atoms. Two and one isomers have been characterized for the imine tautomer and for its amine counterpart, respectively, with the latter species showing a flat conformational landscape.

The synergism between different spectroscopic techniques on the one side and reliable QC calculations on the other allowed us to unravel the role of intrinsic and environmental effects (or, equivalently, inter vs. intra-molecular interactions) in ruling the tautomeric equilibrium of creatinine. The results confirmed that only the amine tautomer can be experimentally characterized either in polar solvents and in the solid state, while both imine and amine tautomers are accessible to gas-phase spectroscopic studies. More generally, the present contribution shows that state-of-the-art QC approaches are suitable to model the different aggregation states of the matter, and are able to fully reconcile theory with experiments. As a matter of fact, by means of vis-à-vis comparisons between experimental and simulated spectra, our integrated strategy can provide a detailed and unbiased atomistic interpretation of the macroscopic molecular behavior.

Experimental Section

Experimental methods

The microwave spectroscopic techniques usually employed in the characterization of biomolecular building blocks exploit an adiabatic expansion of the vaporized sample together with a noble carrier gas. Consequently, conformational relaxation can occur through collisions when the interconversion barrier is low enough,[14,15] with non-proteinogenic amino acids offering a significant example.[16] This explains why an exhaustive search of low-energy minima and an accurate evaluation of their interconversion barriers needs to be carried out to support the experimental work whenever no previous reliable results (as in the present case) are available. To bring creatinine in the gas phase, laser ablation (LA) has been employed. Solid rods of a commercial sample (m.p. = 295 °C) were prepared by pressing the powders with a suitable amount of a commercial binder and successively placed in a dryer for 1 month. The sample was then vaporized in ablation nozzles by means of picosecond Nd:YAG lasers (355 nm, 20 mJ per pulse, 20 ps pulse width) under Ne flow (backing pressure 9 atm) and expanded in the spectrometer cavity.

Measurements were performed with different microwave (MW) spectrometers, namely: (1) chirped pulse (CP) Fourier transform (FT) MW spectrometers (LA-CP-FTMW) working in the 2–8 GHz and 6–18 GHz ranges; (2) molecular beam (MB) FTMW spectrometers (MB-FTMW) working in the 2–8 GHz and 6–18 GHz ranges. While complete accounts on the LA-CP-FTMW and LA-MB-FTMW spectrometers can be found elsewhere[46–48,57–60] and some additional details are reported in the SI, here we mention that, for the LA-CP-FTMW spectrometers, chirped-pulses of 4 μs -directly generated by the 24 Gs/s arbitrary waveform generator- were amplified to about 300 W peak power using a traveling wave tube amplifier.

Infrared (IR) measurements were carried out in a KBr pellet at room temperature by using a Bruker Vertex 70 Fourier-Transform IR (FTIR) spectrometer with a resolution of 2 cm^{-1}.

A detailed account on the experimental methodologies is provided in the SI.

Computational methods

Based on our experience, the following computational strategy has been exploited to analyse the amine/imine tautomerism across the different aggregation states. For the molecular crystal of both tautomers, QC calculations were carried out at the B3LYP–D3[37,39,61] level in conjunction with polarized double-ζ basis sets (see the SI, for details) by making use of periodic boundary conditions to reproduce the periodic environmental pattern. After full geometry optimizations, the infrared (IR) spectrum was computed at the harmonic level. Simultaneously, the IR and Raman spectra of the representative unit of the crystal, i.e., the creatinine dimer, were also calculated.

The aqueous solutions of both tautomers were investigated at the B3LYP–D3/SNSD[62,63] (denoted as B3 along the manuscript) and B2PLYP–D3/maug-cc-pVTZ-dH[34,35,38,39,64] (denoted as B2) levels employing a discrete-continuum model in which the first-shell solvent molecules (five in the present case) were explicitly added to the solute. The resulting complex was embedded in a conductor polarizable continuum model (the model indicated as CPCM) to take bulk solvent effects into the proper account.[43] Raman spectra for the aqueous solution were then computed. Next, water molecules were removed in a stepwise manner to analyse their specific role in tuning the tautomeric equilibrium.

The global PES of the isolated creatinine was fully characterized at the B3 level, followed by the refinement of the structures and harmonic force fields of all stationary points at the B2 level. The latter QC analysis was improved in the electronic energy evaluation of the most significant low-energy minima and the TSs ruling their interconversion (vide infra) by exploiting the so-called "cheap" composite scheme[10,40] (denoted as ChS in the text). Details of the ChS model, which has been demonstrated to perform well for both covalent and noncovalent interactions,[8,17,36] are given in the SI. Once the species suitable for the gas-phase characterization were envisaged, the required spectroscopic parameters were computed, with their equilibrium structures being the key information. Therefore, these were also evaluated by exploiting explicitly-correlated CCSD(T)-F12[41] computations in conjunction with the cc-pVDZ–F12 basis set[42] (in short CCDZF12), which leads – at a much reduced computational cost[65] – to results comparable to those delivered by conventional CCSD(T)[66] computations in conjunction with quadruple-zeta basis sets. Several studies confirm that the selected computational models are able to deliver structural parameters with errors within 0.002 Å and 0.2 degrees for bond lengths and angles, respectively, and energetic quantities with errors within 2 kJ mol^{-1}.[35,36,40]

The periodic calculations for the crystal structure were carried out with the Crystal program,[67] while CCSD(T)-F12 computations were performed using the MOLPRO quantum-chemical package.[68] The GAUSSIAN software[69] was used for all the other calculations. A more detailed account of the computational methodologies is provided in the SI.

Acknowledgements

The authors acknowledge the Flammagroup (www.flammagroup.com) for providing a creatinine sample, Prof. Paolo Stoppa (University Ca' Foscari, Venezia) for support in IR spectra recording, and Mr. Federico Lazzari (SNS) for help with the automatic generation and representation of tautomers. This work has been supported by the Ministerio de Ciencia e Innovación (CTQ2016-76393-P and PID2019-11/1396GB-I00), Junta de Castilla y León (Grants VA077U16 and VA244P20), the European Research Council (ERC-2013-SyG, n. 610256 NANOCOSMOS), MIUR (PRIN 2017, Grant 2017A4XRCA), and by the Italian Space Agency (ASI; 'Life in Space' project, N. 2019-3-U.0).

Conflict of Interest

The authors declare no conflict of interest.

Keywords: laser ablation · quantum chemistry · rotational spectroscopy · tautomerism · vibrational spectroscopy

[1] B. Chandramouli, S. Del Galdo, G. Mancini, N. Tasinato, V. Barone, *Biopolymers* **2018**, *109*, e23109.
[2] T. F. Miller, D. C. Clary, *J. Phys. Chem. B* **2004**, *108* 2484–2488.
[3] D. Boehr, R. Nussinov, P. Wright, *Nat. Chem. Biol.* **2009**, *5*, 789–796.
[4] C. Luchinat, *Phys. Chem. Chem. Phys.* **2016**, *18*, 5684–5685.
[5] G. L. Hofacker, *Intra- and Intermolecular Interactions*, in W. Hoppe, W. Lohmann, H. Markl, H. Ziegler (eds) Biophysics. Springer, Berlin, Heidelberg, **1982**.
[6] M. S. De Vries, P. Hobza, *Annu. Rev. Phys. Chem.* **2007**, *58*, 585–612.
[7] C. Puzzarini, J. Bloino, N. Tasinato, V. Barone, *Chem. Rev.* **2019**, *119*, 8131–8191.
[8] C. Puzzarini, M. Biczysko, V. Barone, I. Peña, C. Cabezas, J. L. Alonso, *Phys. Chem. Chem. Phys.* **2013**, *15*, 16965–16975.
[9] J. Demaison, N. Vogt, Lecture Notes Chem., Springer Nature Switzerland (2020).
[10] C. Puzzarini, M. Biczysko, V. Barone, L. Largo, I. Peña, C. Cabezas, J. L. Alonso, *J. Phys. Chem. Lett.* **2014**, *5*, 534–540.
[11] C. Cabezas, M. Varela, J. L. Alonso, *Angew. Chem. Int. Ed.* **2017**, *56*, 6420–6425; *Angew. Chem.* **2017**, *129*, 6520–6525.
[12] M. Schnell, M. Fatima, C. Perez, A. Steber, S. Zinn, A. Poblotzki, *Angew. Chem. Int. Ed.* **2019**, *58*, 3108–3113; *Angew. Chem.* **2019**, *131*, 3140–3145.
[13] I. Murugachandran, J. Tang, I. Pena, D. Loru, M. E. Sanz, *J. Phys. Chem. Lett.* **2021**, *12*, 1081–1086.
[14] C. Gregory, J. Van Wijngaarden, *J. Mol. Spectrosc.* **2020**, *373*, 111374.
[15] a) R. S. Ruoff, T. D. Klots, T. Emilsson, H. S. Gutowsky, *J. Chem. Phys.* **1990**, *93*, 3142–3150; b) P. D. Godfrey, R. D. Brown, F. M. Rodgers, *J. Mol. Struct.* **1996**, *376*, 65–81.
[16] a) J. L. Alonso, I. Peña, J. C. López, E. R. Alonso, V. Vaquero, *Chem. Eur. J.* **2019**, *25*, 2288–2294; b) A. Simão, C. Cabezas, I. León, E. R. Alonso, S. Mata, J. L. Alonso, *Phys. Chem. Chem. Phys.* **2019**, *21*, 4155–4161.
[17] a) W. Li, L. Spada, N. Tasinato, S. Rampino, L. Evangelisti, A. Gualandi, P. G. Cozzi, S. Melandri, V. Barone, C. Puzzarini, *Angew. Chem. Int. Ed.* **2018**, *57*, 13853–13857; *Angew. Chem.* **2018**, *130*, 14049–14053; b) D. A. Obenchain, L. Spada, S. Alessandrini, S. Rampino, S. Herbers, N. Tasinato, M. Mendolicchio, P. Kraus, J. Gauss, C. Puzzarini, J.-U. Grabow, V. Barone, *Angew. Chem. Int. Ed.* **2018**, *57*, 15822–15826; *Angew. Chem.* **2018**, *130*, 16048–16052; c) J. Wang, L. Spada, J. Chen, S. Gao, S. Alessandrini, G. Feng, C. Puzzarini, Q. Gou, J.-U. Grabow, V. Barone, *Angew. Chem. Int. Ed.* **2019**, *58*, 13935–13941; *Angew. Chem.* **2019**, *131*, 14073–14079.
[18] a) S. Herbers, P. Kraus, J.-U. Grabow, *J. Chem. Phys.* **2019**, *150*, 144308; b) N. Voigt, K. P. Rajappan Nair, J.-U. Grabow, J. Demaison, *Mol. Phys.* **2018**, *116*, 3530–3537.
[19] M.-A. Martin-Drumel, J. H. Baraban, P. B. Changala, J. F. Stanton, M. C. McCarthy, *Chem. Eur. J.* **2019**, *25*, 7243–7258.
[20] M. J. McLeish, G. L. Kenyon, *Crit. Rev. Biochem. Mol. Biol.* **2005**, *40*, 1–20.
[21] R. D. Perrone, N. E. Madias, A. S. Levey, *Clin. Chem.* **1992**, *38*, 1933–1953.
[22] G. L. Myers, W. G. Miller, J. Coresh, J. Fleming, N. Greenberg, T. Greene, T. Hostetter, A. S. Levey, M. Panteghini, M. Welch, J. H. Eckfeldt, *Clin. Chem.* **2006**, *52*, 5–18.
[23] S. Sushrut, S. Waikar, J. V. Bonventre, *J. Am. Soc. Nephrol.* **2009**, *20*, 672–679.
[24] R. K. Cannan, A. Shore, *Biochem. J.* **1928**, *22*, 920–929.
[25] A. R. Butler, C. Glidewell, *J. Chem. Soc. Perkin Trans. 2* **1985**, 1465–1467.
[26] G. L. Kenyon, G. L. Rowley, *J. Am. Chem. Soc.* **1971**, *93*, 5552–5560.
[27] J. S. Craw, S. P. Greatbanks, I. H. Hillier, M. J. Harrison, N. A. Burton, *J. Chem. Phys.* **1997**, *106*, 6612–6617.
[28] J. Gao, Y. Hu, S. Li, Y. Zhang, X. Chen, *Chem. Phys.* **2013**, *410*, 81–89.
[29] Y. Valadbeigi, V. Ilbeigi, M. Tabrizchi, *Comp. Theor. Chem.* **2015**, *1061*, 27–35.
[30] D. Kotsyubynskyy, S. Molchanov, A. Gryff-Keller, *Magn. Reson. Chem.* **2004**, *42*, 1027–1036.
[31] T. W. Bell, Z. Hou, Y. Luo, M. G. B. Drew, E. Chapoteau, B. P. Czech, A. Kumar, *Science* **1995**, *269*, 671–674.
[32] S. Du Prè, H. Mendel, *Acta Crystallogr.* **1955**, *8*, 311–313.
[33] a) K. Vikram, S. Mishra, S. K. Srivastava, R. K. Singh, *J. Mol. Struct.* **2012**, *1012*, 141–150; b) C. Bayrak, S. H. Bayari, *Hacettepe J. Biol. & Chem.* **2010**, *38*, 107–118; c) N. Trendafilova, A. P. Kurbakova, I. A. Efimenko, M. Mitewa, P. R. Bontchev, *Spectrochim. Acta Part A* **1991**, *47*, 577–584.
[34] a) M. Biczysko, P. Panek, G. Scalmani, J. Bloino, V. Barone, *J. Chem. Theory Comput.* **2010**, *6*, 2115–2125; b) R. Boussessi, G. Ceselin, N. Tasinato, V. Barone, *J. Mol. Struct.* **2020**, *1208*, 127886.
[35] T. Fornaro, M. Biczysko, J. Bloino, V. Barone, *Phys. Chem. Chem. Phys.* **2016**, *18*, 8479–8490.
[36] S. Alessandrini, V. Barone, C. Puzzarini, *J. Chem. Theory Comput.* **2020**, *16*, 988–1006.
[37] A. D. Becke, *J. Chem. Phys.* **1993**, *98*, 5648–5652.
[38] S. Grimme, *J. Chem. Phys.* **2006**, *124*, 034108.
[39] a) S. Grimme, J. Anthony, S. Ehrlich, H. Krieg, *J. Chem. Phys.* **2010**, *132*, 154104; b) S. Grimme, S. Ehrlich, L. Goerigk, *J. Comput. Chem.* **2011**, *32*, 1456–1465.
[40] C. Puzzarini, V. Barone, *Phys. Chem. Chem. Phys.* **2011**, *13*, 7189–7197.
[41] T. B. Adler, G. Knizia, H.-J. Werner, *J. Chem. Phys.* **2007**, *127*, 221106.
[42] K. A. Peterson, T. B. Adler, H.-J. Werner, *J. Chem. Phys.* **2008**, *128*, 084102.
[43] a) M. Cossi, N. Rega, G. Scalmani, V. Barone, *J. Comput. Chem.* **2003**, *24*, 669–681; b) A. S. Perera, J. Cheramy, C. Merten, J. Thomas, Y. Xu, *Chem. Phys. Chem.* **2018**, *19*, 2234–2242.
[44] V. Barone, *J. Chem. Phys.* **2005**, *122*, 014108.
[45] J. Bloino, M. Biczysko, V. Barone, *J. Chem. Theory Comput.* **2012**, *8*, 1015–1036.
[46] S. Mata, I. Peña, C. Cabezas, J. C. López, J. L. Alonso, *J. Mol. Spectrosc.* **2012**, *280*, 91–96.
[47] E. R. Alonso, I. León, L. Kolesnivoká, J. L. Alonso, *ChemPhysChem* **2018**, *19*, 3334–3340.
[48] I. Peña, S. Mata, A. Martín, C. Cabezas, A. M. Daly, J. L. Alonso, *Phys. Chem. Chem. Phys.* **2013**, *15*, 18243–18248.
[49] H. M. Pickett, *J. Mol. Spectrosc.* **1991**, *148*, 371–377.
[50] G. G. Brown, B. C. Dian, K. O. Douglass, S. M. Geyer, S. T. Shipman, B. H. Pate, *Rev. Sci. Instrum.* **2008**, *79*, 053103.
[51] D. Schmitz, V. A. Shubert, T. Betz, M. Schnell, *J. Mol. Spectrosc.* **2012**, *280*, 77–84.
[52] I. León, E. R. Alonso, S. Mata, C. Cabezas, J. L. Alonso, *Angew. Chem. Int. Ed.* **2019**, *58*, 16002–16007; *Angew. Chem.* **2019**, *131*, 16148–16153.
[53] I. León, E. R. Alonso, S. Mata, C. Cabezas, M. A. Rodríguez, J.-U. Grabow, J. L. Alonso, *Phys. Chem. Chem. Phys.* **2017**, *19*, 24985–24990.
[54] D. Licari, N. Tasinato, L. Spada, C. Puzzarini, V. Barone, *J. Chem. Theory Comput.* **2017**, *13*, 4382–4396.
[55] Z. Kisiel, L. Pszczółkowski, E. Białkowska-Jaworska, S. B. Charnley, *J. Mol. Spectrosc.* **2007**, *241*, 220–229.

[56] W. Gordy, R. L. Cook, Microwave Molecular Spectra, Wiley, New York, *3rd edn.*, **1984**.
[57] J. L. Alonso, C. Pérez, M. E. Sanz, J. C. López, S. Blanco, *Phys. Chem. Chem. Phys.* **2009**, *11*, 617–627, and references therein.
[58] S. Blanco, M. E. Sanz, J. C. López, J. L. Alonso, *Proc. Natl. Acad. Sci. USA* **2007**, *104*, 20183–20188.
[59] M. E. Sanz, S. Blanco, J. C. López, J. L. Alonso, *Angew. Chem. Int. Ed.* **2008**, *47*, 6216–6220; *Angew. Chem.* **2008**, *120*, 6312–6316.
[60] A. Lesarri, S. Mata, J. C. López, J. L. Alonso, *Rev. Sci. Instrum.* **2003**, *74*, 4799–4804.
[61] J. P. Perdew, K. Burke, Y. Wang, *Phys. Rev. B* **1996**, *54*, 16533–16539.
[62] V. Barone, P. Cimino, E. Stendardo, *J. Chem. Theory Comput.* **2008**, *4*, 751–764.
[63] Double-zeta basis set of SNS family, available in the download section http://smart.sns.it.
[64] E. Papajak, H. R. Leverentz, J. Zheng, D. G. Truhlar, *J. Chem. Theory Comput.* **2009**, *5*, 1197–1202.
[65] P. R. Spackman, D. Jayatilaka, A. Karton, *J. Chem. Phys.* **2016**, *145*, 104101.
[66] K. Raghavachari, G. W. Trucks, J. A. Pople, M. Head-Gordon, *Chem. Phys. Lett.* **1989**, *157*, 479–483.
[67] R. Dovesi, A. Erba, R. Orlando, C. M. Zicovich-Wilson, B. Civalleri, L. Maschio, M. Rérat, S. Casassa, J. Baima, S. Salustro, B. Kirtman, *WIREs Comput. Mol. Sci.* **2018**, *8*, e1360.
[68] H.-J. Werner, P. J. Knowles, G. Knizia, F. R. Manby, M. Schutz, P. Celani, T. Korona, R. Lindh, A. Mitrushenkov, G. Rauhut et al., MOLPRO, version 2020.1, a package of ab-initio programs, **2020**, see http://www.molpro.-net.
[69] M. J. Frisch, G. W. Trucks, H. B. Schlegel, G. E. Scuseria, M. A. Robb, J. R. Cheeseman, G. Scalmani, V. Barone, G. A. Petersson, H. Nakatsuji et al., Gaussian16, Revision C.01, **2016**.

Manuscript received: May 19, 2021
Revised manuscript received: June 22, 2021
Accepted manuscript online: June 23, 2021